Molecular Vision 2018; 24:587-602 <http://www.molvis.org/molvis/v24/587>
Received 7 April 2018 | Accepted 24 August 2018 | Published 27 August 2018

Targeted disruption of the endogenous zebrafish *rhodopsin* locus as models of rapid rod photoreceptor degeneration

Christopher P. Zelinka,[1,2] Mailin Sotolongo-Lopez,[1] James M. Fadool[1,2]

[1]Department of Biological Science, Florida State University, Tallahassee, FL; [2]Program in Neuroscience, Florida State University, Tallahassee, FL

Purpose: Retinitis pigmentosa (RP) is a collection of genetic disorders that results in the degeneration of light-sensitive photoreceptor cells, leading to blindness. RP is associated with more than 70 loci that may display dominant or recessive modes of inheritance, but mutations in the gene encoding the visual pigment rhodopsin (RHO) are the most frequent cause. In an effort to develop precise mutations in zebrafish as novel models of photoreceptor degeneration, we describe the generation and germline transmission of a series of novel clustered regularly interspaced short palindromic repeats (CRISPR)/Cas9-induced insertion and deletion (indel) mutations in the major zebrafish *rho* locus, *rh1–1*.

Methods: One- or two-cell staged zebrafish embryos were microinjected with in vitro transcribed mRNA encoding Cas9 and a single guide RNA (gRNA). Mutations were detected by restriction fragment length polymorphism (RFLP) and DNA sequence analyses in injected embryos and offspring. Immunolabeling with rod- and cone-specific antibodies was used to test for histological and cellular changes.

Results: Using gRNAs that targeted highly conserved regions of *rh1–1*, a series of dominant and recessive alleles were recovered that resulted in the rapid degeneration of rod photoreceptors. No effect on cones was observed. Targeting the 5′-coding sequence of *rh1–1* led to the recovery of several indels similar to disease-associated alleles. A frame shift mutation leading to a premature stop codon (T17*) resulted in rod degeneration when brought to homozygosity. Immunoblot and fluorescence labeling with a Rho-specific antibody suggest that this is indeed a null allele, illustrating that the Rho expression is essential for rod survival. Two in-frame mutations were recovered that disrupted the highly conserved N-linked glycosylation consensus sequence at N15. Larvae heterozygous for either of the alleles demonstrated rapid rod degeneration. Targeting of the 3′-coding region of *rh1–1* resulted in the recovery of an allele encoding a premature stop codon (S347*) upstream of the conserved VSPA sorting sequence and a second in-frame allele that disrupted the putative phosphorylation site at S339. Both alleles resulted in rod death in a dominant inheritance pattern. Following the loss of the targeting sequence, immunolabeling for Rho was no longer restricted to the rod outer segment, but it was also localized to the plasma membrane.

Conclusions: The efficiency of CRISPR/Cas9 for gene targeting, coupled with the large number of mutations associated with RP, provided a backdrop for the rapid isolation of novel alleles in zebrafish that phenocopy disease. These novel lines will provide much needed in-vivo models for high throughput screens of compounds or genes that protect from photoreceptor degeneration.

Retinitis pigmentosa (RP) represents a collection of heritable retinopathies characterized by the progressive degeneration of rod photoreceptors, followed by the secondary loss of cones and circuitry remodeling. RP is associated with mutations at over 70 loci, disrupting not only phototransduction and the visual cycle, but also nearly every aspect of rod cell biology, including development, metabolism, transport, and structure (RetNet). Mutations in rhodopsin (RHO; OMIM 180380) are the most frequent causes of autosomal dominant (ad) RP, and they account for a small fraction of autosomal recessive (ar) RP [1]. More than 150 unique mutations spanning the entire RHO coding sequence have been identified (Human Gene Mutation Database). These mutations disrupt various molecular processes, including phosphorylation, glycosylation, chromophore binding, G-protein activation, arrestin-mediated endocytosis, and targeting of RHO to the rod outer segment (ROS).

RHO mutations have been categorized according to biochemical properties or clinical standards [2-7]. In vitro, class I mutants were defined as showing levels of expression similar to the wild-type (WT) RHO, reconstitution with chromophore, and proper folding; however, in vivo, the protein products mislocalized to the plasma membrane of the cell body [2,3]. These mutations include several at the C-terminus, which disrupt a VXPX consensus sequence necessary for post-Golgi trafficking and the targeting of RHO to the ROS [8]. C-terminal mutations also affect conserved phosphorylation sites essential for protein–protein interactions and the

Correspondence to: James M. Fadool, Department of Biological Science and Program in Neuroscience, Florida State University, 319 Stadium Drive, Tallahassee, FL, 32306; Phone: (850) 644-3550; FAX: (850) 645-8447; email: jfadool@bio.fsu.edu

deactivation of RHO [9]. Class II RHO mutations exhibit reduced expression compared to WT, show poor reconstitution with chromophore, and are retained in the trans-Golgi network, suggesting misfolded or unstable products. These mutations largely alter the 5′ and membrane spanning domains, N-linked glycosylation, or cysteine residues [2]. For example, T17M and RHO P23H, the most common RP allele in the United States [10-14], display retention in the trans-Golgi network [2,3,15] and mutations T4K, T17M, and P23H in or near consensus glycosylation sequences [16-18] alter glycosylation profiles in vitro and similarly affect trafficking. Knowledge of the molecular pathology underlying rod death is incomplete, but these data and mounting evidence suggest that diverse mechanisms are responsible.

Animal models recapitulate many of the histopathological features of RP, and they have been invaluable for investigating the cellular and physiologic consequences of disease-causing mutations. Several of the earliest and frequently exploited rodent models, such as the *rd1*, *rd2*/*rds*, and *rd10* mice [5,19-22] and the Royal College of Surgeons (RCS) rat [23-25], harbor spontaneous mutations in gene orthologs that are associated with human disease. The characterization of transgenic rodent, pig, dog, and frog models overexpressing mutant forms of RHO display reduced or aberrant opsin localization, thinning of the retinal outer nuclear layer (ONL), shortened or dysmorphic ROSs, rod death, and eventually cone death [26-37]. Large animal models, such as canine, with naturally occurring mutations, share common histological features with RP, and they have been incredibly useful for pre-clinical safety testing and recognizing the long-term outcomes of novel therapies [38-42]. In animal models, consistent with the in vitro phenotype of class I mutations, opsin mislocalization precedes progressive photoreceptor death [8,43-46]. Models generated through the knock-in of precise mutations into the endogenous *Rho* locus allow for the probing of highly specific mechanistic hypotheses leading to RP [47-50]. The relative levels of the mRNA expression and protein of the mutant alleles, to those of the WT allele influence the stage of onset and severity of the degeneration phenotype [37]. Other studies demonstrate that a low expression level of P23H RHO was not associated with protein accumulation in the endoplasmic reticulum, but it was appropriately trafficked to the outer segment and altered disc morphogenesis preceded degeneration [48,49]. Advances in gene editing in non-mammalian species open the possibility for expanding the number of animal models harboring precise lesions of RHO to further the understanding of the rod degeneration phenotype. A recent report took advantage of clustered regularly interspaced short palindromic repeats (CRISPR)/Cas9 to target multiple *rho* loci in the tetraploid model *Xenopus laevis*. The data showed that the mutation of a single locus out of three was sufficient to alter rod survival [51].

Zebrafish have proven a powerful forward genetic model for studying retinal development and disease [52-56]. The majority of existing mutations were the product of numerous forward genetic screens to identify genes essential to embryonic development, photoreceptor function, and survival [52-54,57-62]. Those same features of high fecundity, external fertilization, relatively short generation time, and ease of the microinjection of one-cell stage embryos have facilitated the rapid adoption of gene-targeting technologies to test specific hypotheses of gene function in eye development [63-65], to generate reporter knock-ins [66,67], to induce precise modifications through homology-directed repair [68-70], and to model human disease [71,72].

The purpose of this study was to generate zebrafish lines harboring mutations of the major endogenous *rho* locus, *rh1–1*, as models of rod degeneration. Using CRISPR/Cas9, we targeted conserved regions of zebrafish *rh1–1* that are associated with photoreceptor disease in humans. Given the large number of mutations in RHO and the ease and efficiency of gene editing using CRISPR/Cas9, we screened for novel germline mutations of the endogenous locus and then tested for those that phenocopied the rod defects associated with similar mutations in the human locus. This approach offers a strategy for targeting zebrafish genes for functional analyses in vivo, and it provides zebrafish models for investigating the initial cellular changes leading to RP with the potential to develop therapeutic treatments.

METHODS

Animal maintenance: AB strain zebrafish (*Danio rerio*) were reared, bred, and staged according to standard methods [73]. Experiments and procedures were approved by the Florida State University Animal Care and Use Committee. The transgenic (Tg) line *Tg(Xops:EGFP)* expresses enhanced green fluorescent protein (EGFP) in rods under control of the *Xenopus rho* promoter [74]. Animals were anesthetized with MS222 and euthanized in ice water.

CRISPR/Cas9 gene editing: The gRNA plasmids were constructed by the Mutation Generation and Detection Core, University of Utah, to target the 5′ or 3′ coding region of zebrafish *rh1-1*. The gRNA plasmids were PCR-amplified (forward primer: 5′ CAC CGC TAG CTA ATA CGA CTC 3′; reverse primer: 5′ GAT CCG CAC CGA CTC GGT GCC AC 3′) to generate 130 bp in vitro transcription templates including a T7 binding site, 20 nucleotides identical to the 5′ or 3′ *rh1-1*, and a gRNA scaffold sequence. gRNA was

synthesized using the T7 MEGA shortscript kit (Thermo Fisher, Waltham, MA) followed by ethanol precipitation. The 5′ *rh1-1* target sequence 5′ GCC TAT GTC CAA TGC CAC CGG GG 3′ (PAM underlined) 3′ *rh1-1* target sequence: 5′ CCG TGT CTT CCA GCT CCG TGT CT 3′ (PAM underlined) pT3TS-nCas9n plasmid (Addgene #46757, Cambridge, MA) was linearized with *Xba*I followed by phenol-chloroform extraction and ethanol precipitation. A linear plasmid was used as a template for in vitro transcription using the mMESSAGE mMACHINE T3 kit (Thermo Fisher Scientific) and RNA purified using the RNeasy Mini kit (Qiagen, Hilden, Germany). A 1-nl solution containing Cas9 mRNA (200 pg/nl) and one gRNA (100 pg/nl) was microinjected into one- or two-cell staged embryos.

Screening for mutations: DNA was extracted from 20 to 25 injected G_0 embryos or uninjected sibling controls, pooled into groups of five embryos, and used as a template for the PCR amplification of *rh1-1*. For the restriction fragment length polymorphism (RFLP) analysis of 5′ *rh1-1*, a 253-bp product was amplified (forward primer: 5′ ACA GTC CTG CCC AGA CAT CTA 3′; reverse primer: 5′ ATG GTG ACG TAC AGC GTG AG 3′) and digested with *Nci*I (New England Biolabs, Ipswich, MA). Indels were detected by retention of the 253-bp band. For the RFLP analysis of 3′ *rh1-1*, a 325-bp product was amplified (forward primer: 5′ GCG TGG CCT GGT ACA TCT TC 3′; reverse primer: 5′ GGT CTC TGT GTG GTT TGC CG 3′) and digested with *Bbs*I (New England Biolabs). Indels were detected with the gain of a 284-bp band. For the Sanger sequencing analysis, the entire *rh1-1* coding sequence was amplified (1,198 bp, forward primer: 5′ ACA GTC CTG CCC AGA CAT CTA 3′; reverse primer: 5′ GGT CTC TGT GTG GTT TGC CG 3′), purified using the EZNA Cycle Pure kit (Omega Bio-Tek, Norcross, GA), and sequenced with nested primers for 5′ *rh1-1* (5′ ATG GTG ACG TAC AGC GTG AG 3′) or 3′ *rh1-1* (5′ GCG TGG CCT GGT ACA TCT TC 3′).

The remaining injected G_0 embryos were reared to adulthood and outcrossed with WT animals or inbred to generate F_1 fish. DNA was extracted either from F_1 embryos (typically 10–15) or from F_1 adult fin clip tissue and screened for mutations, as described previously.

Histology and imaging: Immunolabeling and fluorescence microscopy of retinal cryosections (10 µm) were performed, as described previously [59,74]. Adults and larvae were genotyped by DNA sequence analysis. The following primary antibodies were used: 1D1 (mouse monoclonal antibody (mab), 1:20) against Rho [74], 4C12 (mouse mab, 1:20) to label the rod plasma membrane [74], and Zpr-1/FRet 43 (mouse mab, 1:20) against Arr3a to label double cone cells [75,76]. Species-specific Alexa-conjugated secondary antibodies were from Molecular Probes (Thermo Fisher). Sections were imaged using either a Zeiss Axiovert S100 fluorescent microscope or a Zeiss LSM 510 Laser Confocal equipped with a 40X C-Apochromat water immersion objective (NA 1.2).

Terminal deoxynucleotide transferase (TdT)-mediated dUTP nick-end labeling (TUNEL) assay was performed on retinal cryosections using the In Situ Cell Detection kit (TMR red, Roche, Basel, Switzerland), as per the manufacturer's protocol, and co-labeled for rods (4C12).

SDS-Page and immunoblot analysis: Immunoblotting was performed as previously described [77,78] with the following modifications. Three individuals of each genotype were used for the analysis. Two retinas from an adult fish were dissected in cold 80% Hanks salt solution, pooled and homogenized in 50 mM of Tris-buffered saline containing 0.5% Triton X-100 and a protease inhibitor cocktail, and incubated for 3 h at 4 °C. Insoluble material was pelleted by centrifugation at 12,000 ×g. In total, 10 µg of the soluble protein per sample was diluted in a sodium dodecyl sulfate (SDS) gel-loading buffer and separated on 12% acrylamide gels by SDS–polyacrylamide gel electrophoresis (PAGE), followed by electrotransfer to nitrocellulose. Duplicate blots were immunolabeled with the 1D1 mab against Rho diluted at 1:1,000 in a blocking buffer or the mouse anti-B-actin mab (Cat# A2228; Sigma-Aldrich, St. Louis, MO) diluted at 1:1,000, followed by peroxidase-conjugated goat anti-mouse secondary antibody (Sigma-Aldrich) diluted at 1:3,000. Labeling was detected using enhanced chemiluminescence (ECL; GE Health Life Sciences, Marlborough, MA) with exposure on Fugi Rx film (MIDSCI, St. Louis, MO). Quantitative densitometry of immunolabeling was performed using a Hewlett-Packard Scanner (model Scanjet 4850; Hewlett Packard, Palo Alto, CA) in combination with Quantiscan software (Biosoft, Cambridge, UK; 78). Rho labeling was standardized to actin labeling as an internal control. Standardized immunodensity values were then compared across genotypes using the Kruskal–Wallis statistical analysis with a significance value of $p<0.05$.

RESULTS

CRISPR/Cas9 targeted mutagenesis of zebrafish rho: Our goal was to generate lines of zebrafish harboring mutations of *rh1–1* that mimic disease-causing alleles in humans. In zebrafish, *rh1–1* is located on chromosome 8. As in other teleosts, the gene is represented by a single exon (Figure 1A), but the protein sequence shares considerable homology with other vertebrate RHO proteins (Figure 1B). A second *rho* gene, *rh1–2*, is located on chromosome 11, but RNA in

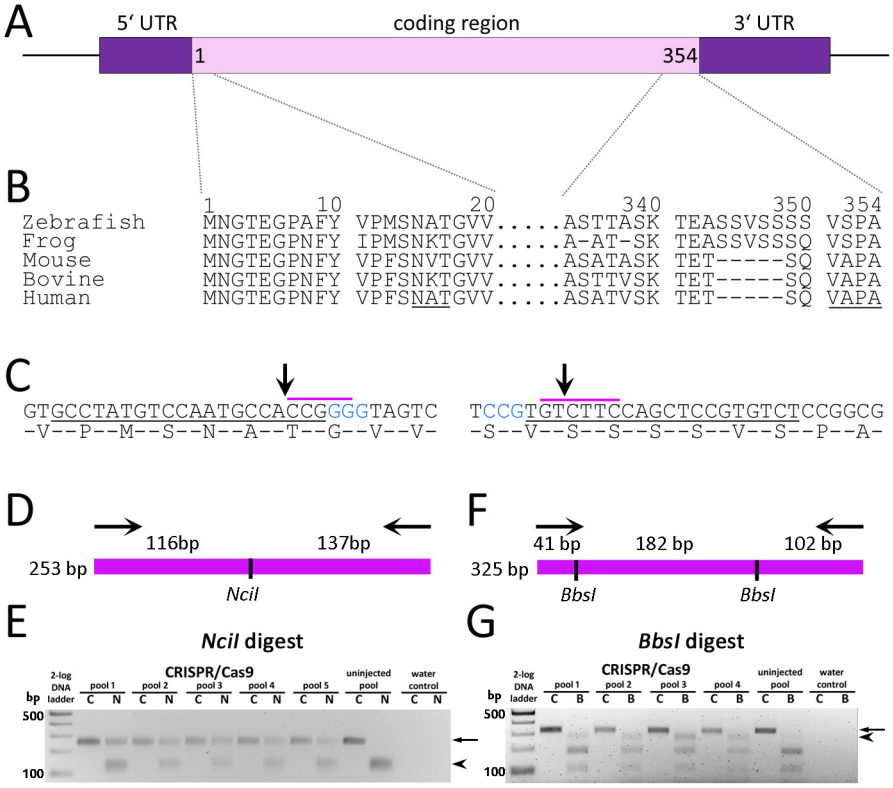

Figure 1. Gene targeting of zebrafish *rh1-1*. **A**: Schematic representation of the zebrafish *rh1-1* locus characterized by a single exon encoding 354 amino acid proteins and 5′ and 3′ UTRs. **B**: Alignment of Rho N- and C-terminal amino acid sequences across species. Numbering is based on the predicted zebrafish *rh1–1*. The conserved N-linked glycosylation sequence and VXPX targeting sequence are underlined. **C**: DNA sequence and amino acid overlay of zebrafish *rh1–1* 5′- (left) and 3′- (right) coding sequences. Blue text represents the CRISPR PAM sequence. Underlined DNA represents the target for guide RNA hybridization. The purple overscore represent restriction sites for *Nci*I or *Bbs*I. Arrows indicate predicted Cas9 cleavage sites. **D**: Diagrammatic representation of the 253-bp 5′- *rh1–1* gene amplicon and the predicted products following digestion with *Nci*I. **E**: RFLP analysis of a 253-bp PCR product spanning the 5′ *rh1–1* gene (C, undigested control) and digested with *Nci*I (N) shows retention of the original amplicon (arrow) from pooled DNA from injected embryos versus complete digestion of the PCR product of uninjected control DNA (arrowhead). **F**: Diagrammatic representation of the 325-bp 3′-amplicon and the predicted products following digestion with *Bbs*I. **G**: RFLP analysis of a 325-bp PCR product (C, undigested control) spanning the 3′ *rh1–1* sequence digested with *Bbs*I (B). The PCR product (arrow) from uninjected-controls was digested to near completion, yielding two visible bands of 102 and 182 bp. The 284-bp band (arrowhead) following loss of the 5′-*Bbs*I site is clearly visible in the injected embryos relative to the controls. The following sequences were used for the RHO alignment: *Danio rerio* (NP571159.1), *X. laevis* (NP001080517.1), *Mus musculus* (NP663358.1), *Bos taurus* (NP001014890.1), and *Homo sapiens* (NP000530.1).

situ hybridization shows a spatially and temporally restricted pattern of expression [79,80]; therefore, we focused more effort on *rh1–1*. Zebrafish *rh1–1* was targeted for disruption using CRISPR/Cas9 and gRNA targeting PAM sequences near conserved motifs in the 5′- and 3′-coding sequences (Figure 1C). One- or two-cell staged zebrafish embryos were microinjected with in vitro transcribed mRNA encoding Cas9 and a single gRNA complementary to either the 5′ *rh1–1* region encoding the N-linked glycosylation consensus sequence at N15 or the 3′ *rh1–1* region just upstream of the sequences encoding VSPA intracellular trafficking moiety. At 24 h post-fertilization (hpf), DNA was extracted from injected embryos and uninjected controls and used as a template for PCR. The efficiency of the gRNA and Cas9 pair was analyzed by RFLP analysis (Figure 1D-G) and validated by Sanger sequencing. Targeting the 5′-region of *rh1–1*, indels were detected by the loss of an *Nci*I restriction site and retention of the 253-bp amplicon (Figure 1D,E arrow). Alterations to the chromatograms were consistent with mosaicism in the template DNA sequence starting at the predicted Cas9 cleavage site (data not shown). Indels at 3′ *rh1–1* were detected following digestion of a 325-bp 3′-*rh1–1* amplicon with *Bbs*I by the gain of a 284-bp band (Figure 1F,G). Baseline noise in the chromatograms downstream of the Cas9 cleavage site was interpreted as a low level of mosaicism (data not shown).

To identify the germline transmission of mutant *rh1–1* alleles, clutches of injected embryos were grown to adults. G_0 adults were inbred or outcrossed to uninjected animals. DNA isolated from F_1 embryos was screened by RFLP and Sanger sequencing, as described above. The germline transmission of novel alleles affecting both targeted regions was readily identified in the F_1 consistent with the mosaicism observed in the chromatograms of injected embryos. F_1 progeny were grown to adults and genotyped by fin clipping to identify specific

rh1–1 alleles. Four mutations in the 5′-coding sequence and six mutations in the 3′-coding sequence were recovered, including in-frame deletions and a putative null allele (Table 1). The phenotypes for five of the alleles are described below. All analyses were performed on larvae from multiple generations, and the phenotypes did not vary across generations.

Disruption of zebrafish N-terminal Rho causes rod degeneration: The zebrafish *rho*^{fl6} allele encodes a non-sense mutation at codon 17 (T17*), predicted to form a truncated product or a null allele (Figure 2A). If a null allele, it is anticipated that heterozygous animals will express approximately half of the level of Rho as WT animals [81]. Therefore, we compared the level of the Rho expression in retinas from heterozygous *rho*$^{fl6/+}$ and homozygous *rho*$^{fl6/fl6}$ fish to that of WT adults (n=3 for each genotype). Immunolabeling for Rho using the 1D1 mab was detected as a ladder with major bands at 32, 64, and 98 kDa (Figure 2B). The densitometry of the immunoblots indicated that Rho labeling was significantly different ($p<0.025$, Kruskel-Wallace test) in heterozygous *rho*$^{fl6/+}$ and homozygous *rho*$^{fl6/fl6}$ samples compared to homozygous WT samples, with approximately half the labeling in the heterozygotes and virtually no detectable labeling in the homozygous *rho*$^{fl6/fl6}$ retinas, consistent with *rho*^{fl6} being a null allele (Figure 2C).

Differential immunolabeling of a histological section with the 1D1 mab and the 4C12 mab, which recognizes an epitope on the rod plasma membrane [74], allowed for the analysis of rod presence independent of the opsin expression. Sections of 5 or 6 dpf WT larvae immunolabeled with 1D1, 4C12, or Zpr-1 were consistent with the previously described arrangement of rods and cones across the ONL. Immunolabeling with either 4C12 or 1D1/Rho showed the typical asymmetric patterning of rods with the greatest intensity of labeling in the ventral retina and more sparse cells in the central and dorsal retina (Figure 2D,E). 1D1 selectively labels the outer segment and 4C12 labels the entire rod photoreceptor, revealing the position of their cell bodies at the innermost region of the ONL. Of the four cone subtypes, red and green wavelength-sensitive cones can be immunolabeled with the Zpr-1 mab, which recognizes Arr3a [75,76]. Immunolabeling for cones shows uniform palisades across the length of the ONL (Figure 2D,E). Rod and cone distributions in heterozygous *rho*$^{fl6/+}$ larvae appear similar to those in the WT. In homozygous *rho*$^{fl6/fl6}$ retinas, Rho immunostaining is completely absent, but the immunolabeling of rods was observed close to the retinal margin (Figure 2 D,E), the site of continual neurogenesis in teleosts [82]. These data are consistent with *rho*$^{fl6/fl6}$ as a likely null allele. Furthermore, the lack of rod immunolabeling in the central retina suggests the Rho expression in zebrafish is essential for rod survival. Labeling of red/green cones in *rho*$^{fl6/fl6}$ was indistinguishable from that of the WT, indicating that the genetic alteration resulted in a rod-specific defect.

Two of the N-terminal mutations were predicted as in-frame alterations that disrupt an N-linked glycosylation consensus sequence (Figure 3A). The N-linked glycosylation of proteins occurs at NXS/T consensus sequences, where X can be any amino acid other than proline. Human mutations at N15 and T17 disrupt a conserved glycosylation sequence and are associated with adRP. The zebrafish *rho*^{f10} and *rho*^{f17} alleles disrupt the conserved consensus sequence that includes N15 (Figure 3A,C). Zebrafish *rho*^{f10} encodes an in-frame deletion of T17 while leaving the remaining coding sequence unaltered (Figure 3A). The zebrafish *rho*^{f17} allele deletes both A16 and T17 and inserts a proline at codon 16 (Figure 3C). WT siblings immunolabeled for rod and cone markers at 6 dpf display the expected labeling across the ONL (Figure 3B,D). In heterozygous *rho*$^{f17/+}$ and *rho*$^{f110/+}$ larvae, rod and Rho immunolabeling is confined to the peripheral retinas, with no labeling of the central retina. Immunolabeling for cones was unaltered from the controls (Figure 3B-E). The phenotype of the heterozygous and homozygous mutants was similar with labeling restricted to the retinal margin.

Disruption of zebrafish C-terminal Rho causes rod degeneration: Several alleles were recovered using a gRNA that targeted Cas9 to a site just upstream of the DNA encoding the conserved VSPA sorting sequence and phosphorylation sites. The zebrafish *rho*^{fl8} allele results in an in-frame deletion of A338 and S339, as well as the insertion of T338, V339, W340, and T341, disrupting a putative phosphorylation site at S339 (Figure 4A). Similar to that observed for previous alleles, immunolabeling of 6 dpf retinal sections for Rho and rods was limited to a few cells near the retinal margin, whereas the red/green cones remained intact (Figure 4C).

The zebrafish *rho*^{fl9} allele results in a non-sense mutation at codon 347 (S347*), eliminating the final eight amino acids of the Rho C-terminal tail, including the conserved VXPX targeting signal (VAPA in humans, VSPA in zebrafish; Figure 1B). Heterozygous *rho*$^{fl9/+}$ larvae display loss of rods and Rho staining from the central retina, with no obvious effect on the immunolabeling of red/green cone photoreceptors (Figure 4C). In humans, rodents, and frogs, disruption of the C-terminal VXPX consensus sequence results in the mistrafficking of Rho to the plasma membrane [8,9,43-46]. To determine whether the *rho*^{fl9} mutation in zebrafish disrupts Rho trafficking, the *rho*^{fl9} was placed on the *Xops:EGFP* reporter line background. The EGFP expression fills the entire rod cell body, terminals, inner segment, and, to a lesser extent,

Table 1. Frequency of and rhodopsin mutations recovered in F1 following gene targeting in zebrafish.

Target	Transmitting G_0 adults/No. tested	Mutations recovered in F1	Allele	DNA sequence	Predicted Mutation
5′ *rho*, codon 17	2/5 (40%)	4	*rho*^{WT}	GCCTATGTCCAATGCCACCG*GGG*TAGTC	
			rho^{fl6}	GCCTATGTCCAATGCC**T**A**ACCCTAAC**CCG*GGG*TAGTC	p.T17*
			rho^{fl7}	GCCTATGTCCAAT---CC**G**G*GGG*TAGTC	p.A16_T17delinsP
			rho^{fl10}	GCCTATGTCCAATG---CCG*GGG*TAGTC	p.T17del
			-	GCCTATGTCCA---------AGTC	-
3′ *rho*, codon 347	3/7 (43%)	6	*rho*^{WT}	ACCGCCTCCAAGACCGAGGCTTCGT*CCG*TGTCTTCCAGCTCCGTGTCTCCGGCGTAAA	
			rho^{fl8}	ACC**A**C-T**GTCTGG**A-CG----AAGACCGAGGCTTCGTCCGTGTCTTCCAGCT*CC-G*TGT	p.A338_S339delinsTVWT
			rho^{fl9}	ACCGCCTCCAAGACCGAGGCTTCGT*CCG*TGT----------AAA	p.S347*
			-	ACCGCCTCCAAGACCGAGGCTTCGT*CCG*T----------AAA	-
			-	ACCGCCTCCAAGACCGAGGCTTCGT*CCG*TGTCTTCCAG----------	-
			-	ACCG------AGGCTTCGTCCGTGTCTTCCAGCT*CCG*TGTCTCCGGCGTAAA	-
			-	ACCGCCTCCAAGACCGAGGCTTCGT*CCG*----------GCGTAAA	-

Sequence analysis and frequency of germ line transmission of 5′ *rho* and 3′ *rho* CRISPR/Cas9-induced alleles aligned to the wild-type *rho* allele (WT) show that the majority represents deletions and insertions (bold text). Italics text represents CRISPR PAM sequence. Underlined DNA represents gRNA target sequence. Alleles characterized in this report are indicated by an allele designation.

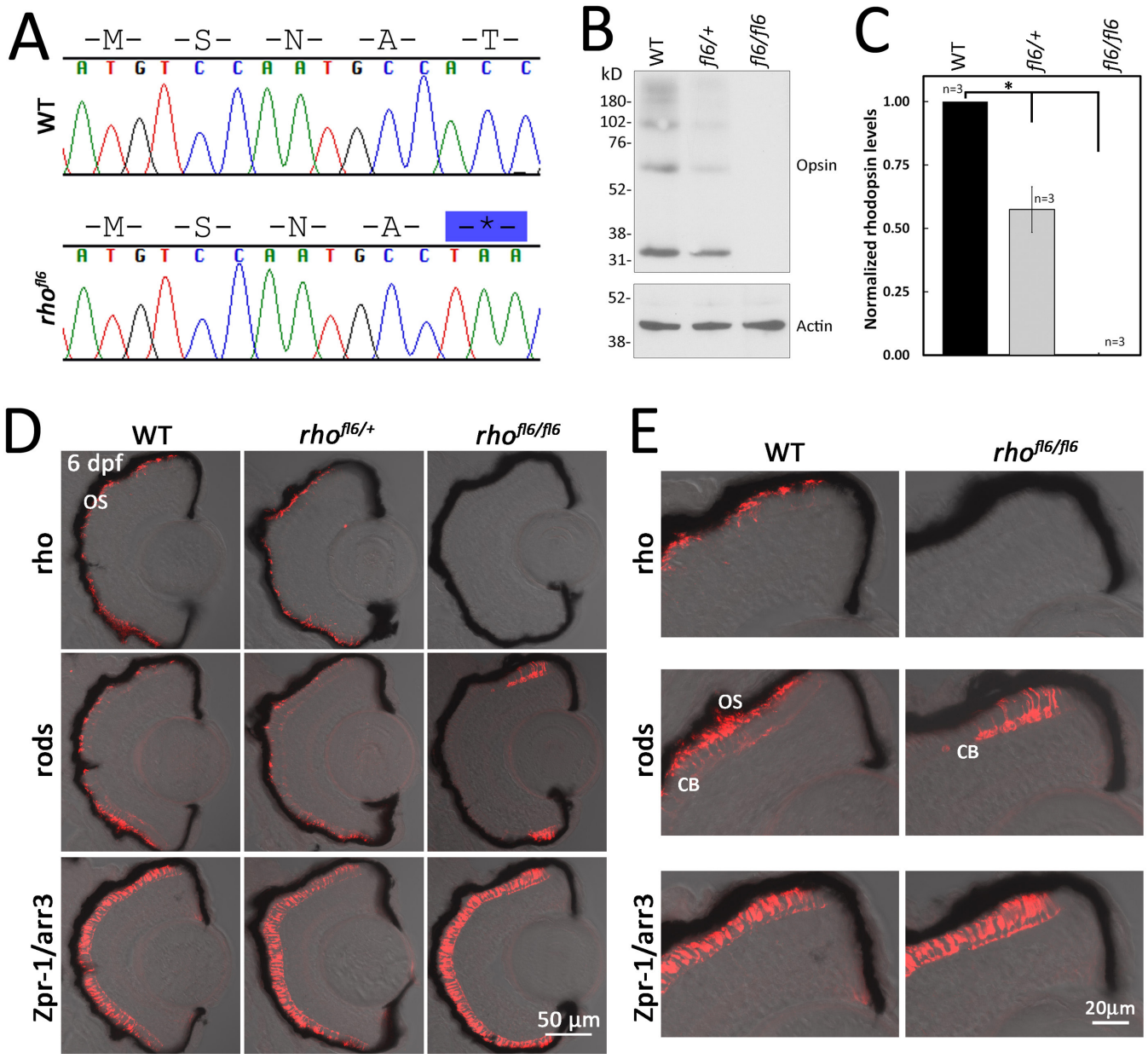

Figure 2. DNA sequence and histology of *rho*^{fl6} encoding a premature stop codon p.17T*. **A**: Chromatograms overlaid with amino acid sequences comparing WT and *rho*^{fl6} allele encoding p.17T*. **B**: Representative immunoblot analysis of detergent-soluble extracts of retinas from WT, heterozygous *rho*$^{fl6/+}$, or homozygous *rho*$^{fl6/fl6}$ adults separated by SDS–PAGE, transferred to nitrocellulose, and probed with the 1D1 mab against Rho or mab AC-74 against B-Actin. Immunolabeling of opsin observed as the monomer at 32 kDa and multimers at 64, and 98 kDa were reduced in the heterozygous *rho*$^{fl6/+}$ sample and not detected in the homozygous *rho*$^{fl6/fl6}$ retina. **C**: Bar graph of normalized densitometry of immunoblot labeling for Rho (n = 3 animals per genotype), * p<0.025, Kruskal-Wallis test. **D**: Confocal images of cryosections of retinas from 6 dpf WT, heterozygous *rho*$^{fl6/+}$, or homozygous *rho*$^{fl6/fl6}$ mutants labeled with antibodies to Rho (1D1, red), rods (4C12, red), or Zpr-1/Arr3a, a selective marker expressed by red/green cones (Zpr-1, red) overlaid with bright-field microscopy. Note the lack of labeling for rods in the central retina and differential labeling for Rho/1D1 and rods/4C12 near the retinal margin of *rho*$^{fl6/fl6}$ homozygous larvae, suggesting that *rho*^{fl6} is a null allele. **E**: Higher magnification images of immunolabeling of the dorsal retinal margin WT and homozygous *rho*$^{fl6/fl6}$ mutants showing the lack of immunolabeling for Rho, an absence of outer segments (OS), but labeling of the cell bodies (CB) by 4C12 in the homozygous mutant larvae.

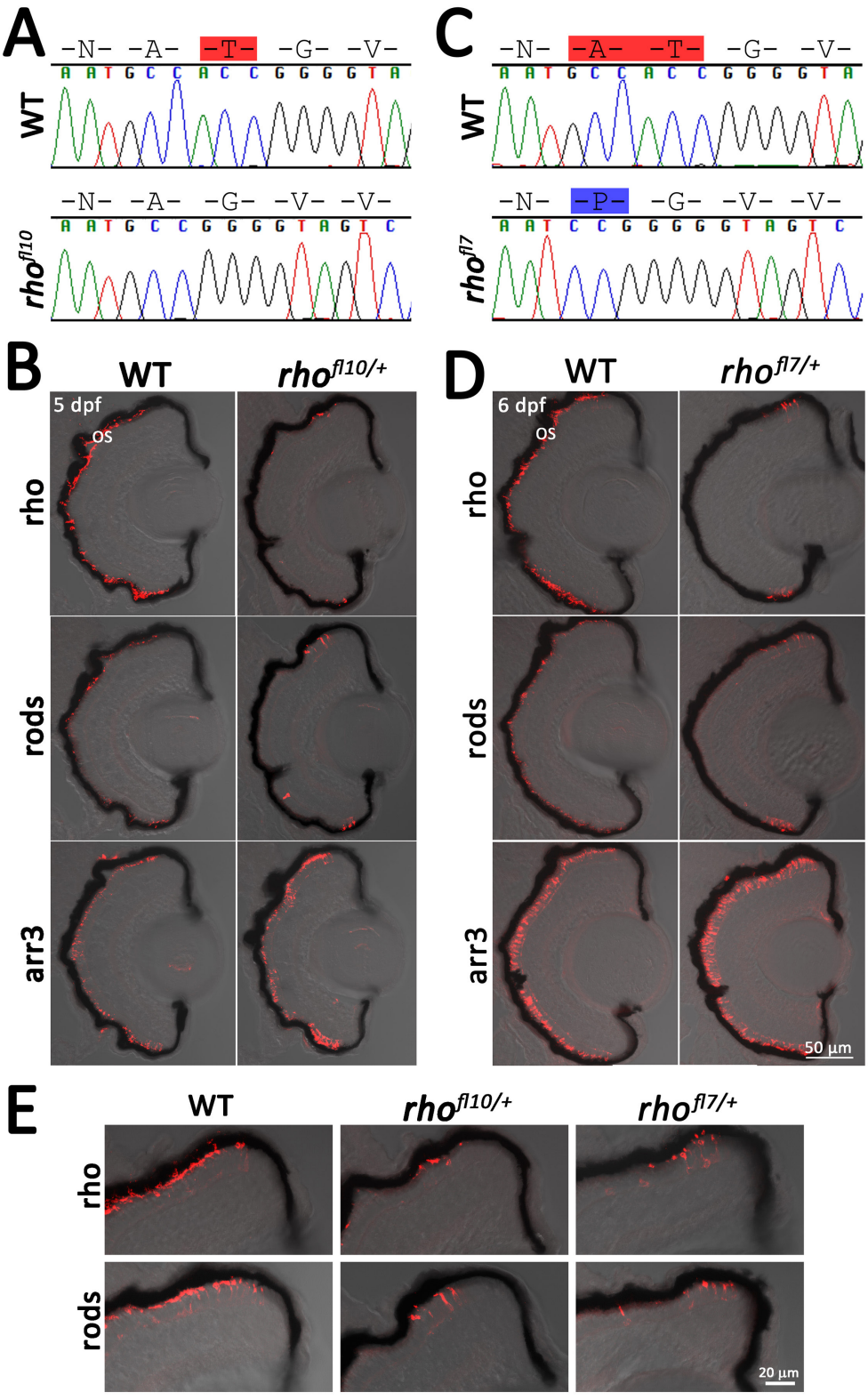

Figure 3. Disruption of the N-linked glycosylation sequence in *rho*^{fl10} and *rho*^{fl7} leads to rod degeneration. **A, C**: Chromatograms overlaid with amino acid sequences comparing WT, *rho*^{fl10}, and *rho*^{fl7} alleles, disrupting the conserved NXT consensus glycosylation sequence at N15. Red highlights deleted amino acids, while blue highlights insertions. **B, D**: Confocal images of serial retinal cryosections of 5 or 6 dpf WT or heterozygous *rho*$^{fl10/+}$ and *rho*$^{fl7/+}$ mutants labeled with antibodies to Rho (1D1, red), rods (4C12, red), and Arr3a (Zpr-1, red) overlaid with bright-field microscopy reveal loss of rod-specific labeling in the central retina. **E**: Higher magnification images of the dorsal retinal margin from WT, heterozygous *rho*$^{fl10/+}$, or *rho*$^{fl7/+}$ mutants showing sparse immunolabeling for Rho and rods.

the outer segment [74]. In WT siblings, immunolabeling for Rho specifically localizes to the outer segment (Figure 4D). However, in *rho*$^{fl9/+}$ heterozygous animals, immunolabeling for Rho was not restricted to the outer segment, but localized to the plasma membrane of the cell body, and many rods lack overt labeling of an outer segment (Figure 4D).

Rho mislocalization and cell death in adult zebrafish with N- and C-terminal Rho mutations: The fact that in zebrafish, rods are not essential for viability allows for the analysis of phenotypes in adults carrying *rh1–1* mutations. The extent of the changes in the number and morphology of the rods in *rho*$^{fl7/+}$ and *rho*$^{fl9/+}$ adult retinas were clear following immunolabeling with the 4C12 mab (Figure 5A-C). At this age in WT retinas, the photoreceptor cell nuclei are tiered with rod cell bodies, forming a row of several cells in thickness vitread to the elongated cone nuclei (Figure 5A). The rod inner segments project distally past the row of cone nuclei, and the outer segments interdigitate with the pigmented epithelium (Figure 5A). In *rho*$^{fl7/+}$ (Figure 5B) and *rho*$^{fl9/+}$ (Figure 5C) retinas, fewer rods were present, their spacing and morphologies were less regular, and no outer segments were labeled. In both mutants, TUNEL was observed in the ONL adjacent to the OPL (arrows, Figure 5B,C), but no TUNEL was observed in WT retinas (Figure 5A). Immunolabeling for Rho confirmed the lack of outer segments and altered trafficking in *rho*$^{fl7/+}$ and *rho*$^{fl9/+}$ adult retinas. In WT adults, immunolabeling of Rho was restricted to the outer segments located at the most distal region of the retina that interdigitate with the pigmented epithelium (Figure 5D, top of the panel). In heterozygous *rho*$^{fl7/+}$ or *rho*$^{fl9/+}$ adults, the rod cell bodies were immunolabeled for Rho, and little outer segment material was observed (Figure 5E,F). Immunolabeling for red and green cones (Figure 5G-I) showed no differences between WT and mutant samples.

DISCUSSION

This study reports the characterization of novel zebrafish models of rod degeneration produced by the CRISPR/Cas9 gene disruption of two separate targets within the *rh1–1* gene. We isolated alleles that behave as disease-causing mutations observed in the clinic and in other well-characterized animal models. We showed evidence that N-terminal and C-terminal mutations resulted in rapid rod degeneration in larval zebrafish; however, similar to our previous report [59], the loss of rods did not appear to affect cones in adults up to 7 months of age. The goal in targeting the endogenous zebrafish locus is that the alleles will recapitulate transcriptional regulation, mRNA processing, and post-translational modifications, which may underlay the variation in the onset of visual deficits observed in clinically relevant disease alleles. Ultimately, these lines in zebrafish will provide much-needed models for high throughput genetic and small molecule screens in an effort to identify compounds or pathways that may lessen the initial pathological sequences leading to rod degeneration.

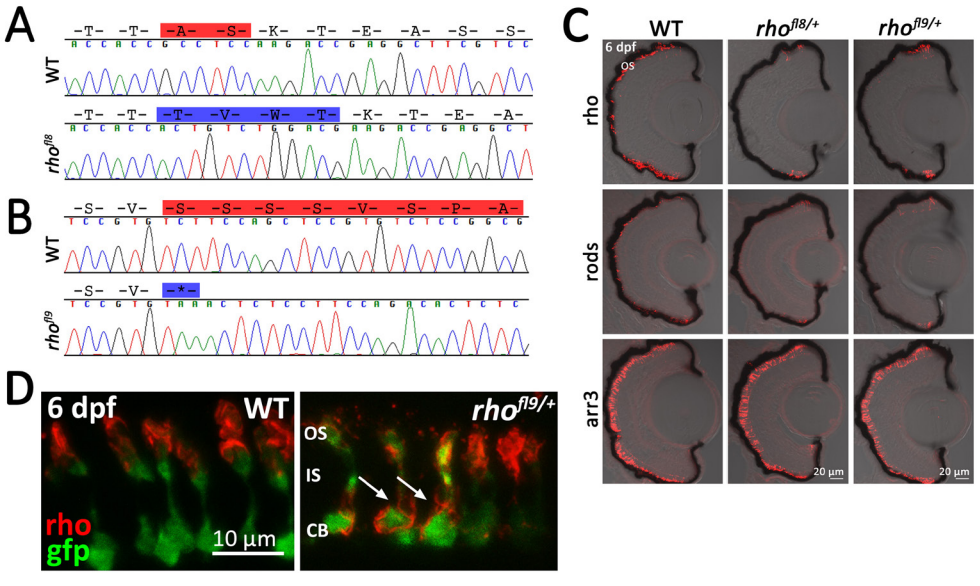

Figure 4. Alteration of conserved C-terminal domains in *rho*^{fl8} *and* *rho*^{fl9}. **A, B**: Chromatograms overlaid with amino acid sequences of 3′ *rh1-1* in WT, the *rho*^{fl8} allele, and the *rho*^{fl9} allele. Predicted amino acid deletions are highlighted in red on the WT sequences; insertions are highlighted in blue on the mutant sequence. **C**: Confocal images of retinal sections of 6 dpf WT or heterozygous *rho*$^{fl8/+}$ or *rho*$^{fl9/+}$ larvae labeled with antibodies to Rho (1D1, red), rods (4C12, red), or Arr3a (Zpr-1, red) overlaid with bright-field microscopy. **D**: High magnification confocal images of 6 dpf WT or heterozygous *rho*$^{fl9/+}$ larvae showing the rod-specific expression of EGFP (gfp, green) and immunolabeling for Rho (1D1, red). In WT retinas, the Rho immunolabeling is localized to the outer segment (OS), while in the mutant, Rho immunolabeling is localized to the inner segment (IS) and the cell body (CB; arrows).

TALENs and CRISPR/Cas9 have opened the door to the development of a range of innovative tools and approaches to study gene function in vitro and in vivo. While many have taken advantage of the ability to tag genes with reporter knock-ins [66,67] or to induce precise modifications through homology-directed repair [68-70], we took a relatively simpler approach to isolate novel germline mutations and retain those that have phenocopied mutations of the human locus. Given the ease and efficiency of gene editing in zebrafish using CRISPR/Cas9, an extension of the approach is that gRNAs could be designed to tile any region of a gene to induce a library of in-vivo mutations to screen for effects on gene function or novel phenotypes.

The targeted disruption of 5′ *rh1–1* yielded a putative null allele, *rho*^{fl6}, and two alleles, *rho*^{fl7} and *rho*^{fl10}, encoding in-frame mutations and altering the conserved NXT glycosylation consensus sequence at N15. *rho*^{fl7} removes XT and inserts a proline, whereas *rho*^{fl10} deletes T17. In heterozygous larvae, both alleles result in rod-specific cell death and a reduced opsin expression. Human mutations N15S and T17M affecting the N15 RHO glycosylation consensus sequence are associated with adRP [17,18]. RHO N15S and T17M alleles are classified as class II mutations, which are expressed at lower levels than WT opsin, fail to reconstitute with chromophore, and are retained in the trans-Golgi network in heterologous in-vitro expression systems [2-4]. Transgenic animal models overexpressing these class II adRP alleles exhibit shortened ROSs, ONL thinning, and rod death [30,36], confirming that glycosylation at N15 is essential.

The putative null allele, *rho*^{fl6} (T17*), is the only mutation in our set that results in a recessive phenotype. A reduced expression by immunoblot and differential immunolabeling with the Rho-specific mab and a mab that labels an antigen expressed on the rod plasma membranes and the outer segment confirm that this is a null allele. While most human RHO mutations cause adRP, several alleles result in arRP, including null alleles of RHO [44,83,84]. Similar to null alleles in humans and mice [82,85-87], homozygous *rho*^{fl6} zebrafish exhibit rod degeneration consistent with the opsin expression being essential for rod survival, whereas heterozygous animals display no rod death but lower levels of immunolabeling by the Rho-specific antibody. Multiple polymorphisms at each V345 and P347, as well as deletion of the distal RHO C-terminus (Q344ter) likely affect vectorial

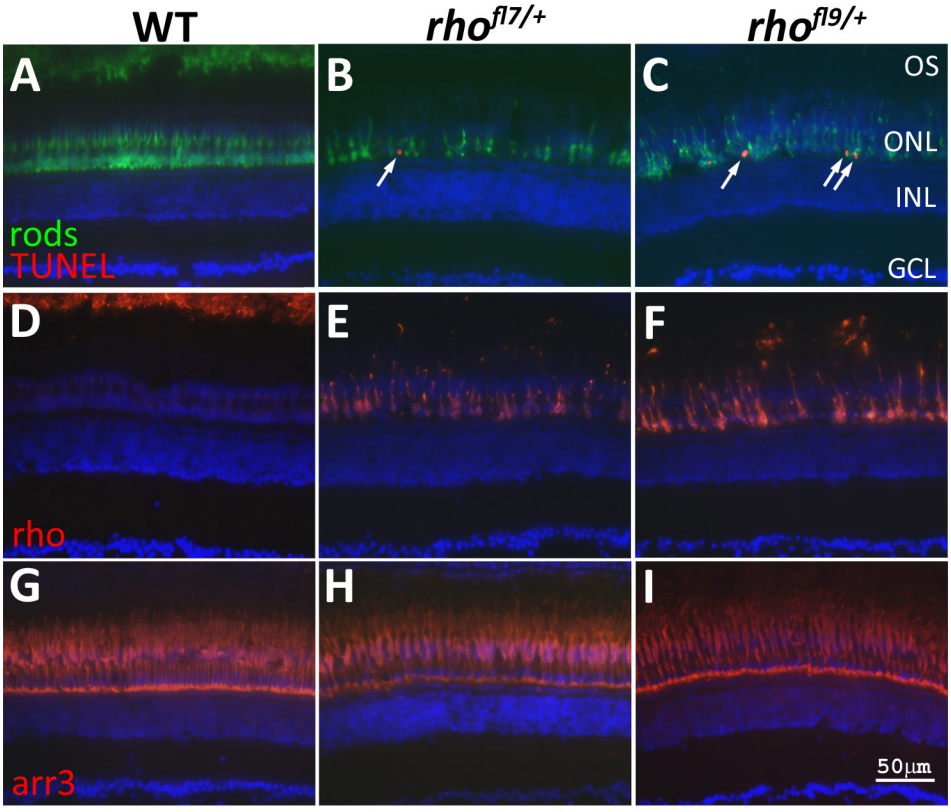

Figure 5. *rho*^{fl7} and *rho*^{fl9} lead to increased TUNEL in adults. Retinal sections of WT (**A,D,G**) or heterozygous *rho*$^{fl7/+}$ (**B,E,H**) and *rho*$^{fl9/+}$ (**C,F,I**) adult zebrafish immunolabeled with antibodies to rods (4C12, green, **A-C**), Rho (1D1, red, **D-F**), or red/green cones (Arr3a/Zpr-1, red, **G-I**) and stained with TUNEL (red, **A-C**). All sections were counterstained with DAPI (blue). Immunolabeling for rods reveals fewer, less regularly arranged cells in the mutants compared to the WT. TUNEL-positive nuclei (arrows), positioned along the proximal region of the ONL, are only observed in the mutant retinas **(A-C)**. In WT retinas, Rho immunolabeling is restricted to the ROS at the top of the panel **D**. Immunolabeling in *rho*$^{fl7/+}$ and *rho*$^{fl9/+}$ adults is localized to the cell bodies, and no outer segments are evident (**E-F**). Immunolabeling for red and green cones was indistinguishable across the samples (**G-H**). Abbreviations: ganglion cell layer, GCL; inner nuclear layer, INL; outer nuclear layer, ONL.

sorting of RHO to the ROS [8,9]. Disruption of a putative phosphorylation site at S339 *rho*^{fl8} results in rod death and the lack of the full VXPX sorting signal (*rho*^{fl9}) exhibits opsin mislocalization, consistent with mouse, rat, rabbit, frog, and pig models [9,42-45]. In all, the cones appear unaltered consistent with our previous report [59], which has allowed for an analysis of regeneration and circuitry remodeling in the absence of cone death [58-61].

The rapid rod degeneration observed in the *rh1–1* mutant zebrafish described in this report compared to other animal models and human RP is notable. Regardless of the lesion, mutations of the endogenous zebrafish *rh1–1* result in a lack of rod labeling in the central and ventral retina by 6 dpf. Rod-specific labeling was limited to the retinal margin, the site of continuing retinal neurogenesis in teleosts [81]. This pattern of cell death is similar to that observed in a transgenic line of zebrafish overexpressing a membrane-targeted CFP (mCFP) in rod photoreceptors [59]. Overexpression of mCFP under the control of the *Xenopus* opsin promoter resulted in Rho mislocalization to the plasma membrane and the retention of a Rho–GFP fusion protein in the endoplasmic reticulum or Golgi [59]. It remains unclear what underlies the more rapid rod degeneration in zebrafish models. In mice and rats, data suggest that variation in the rate of photoreceptor degeneration may be dependent on the copy number of the mutant opsin transgene or the relative amount or ratio of the mutant to WT Rho expressions [45,50]; however, only the most aggressive rodent models show similar rapid cell death. One possibility is that the swift death observed in our models may be a consequence of the pace of differentiation in the rapidly developing zebrafish larvae. In zebrafish embryos and during photoreceptor regeneration, the expressions of the transcription factors Crx, Nrl, and Nr2e3 precede terminal mitosis, and final cell division is symmetric, generating two cells of the same photoreceptor subtype [60,88-90], suggesting that neuroblasts are primed for rapid differentiation. The *rho* expression first appears in the ventral retina between 50 and 52 hpf, a time frame within hours of terminal mitosis [76,90-94]. Rod numbers increased rapidly within the ventral retina, and they extended into the nasal and temporal regions of the retina by 70 hpf [90,92,93]. The first outer segments appear at 60 hpf [95,96], and larvae exhibit their first visual responses at approximately 70 hpf [97,98]. Taken together, the rapid onset and high level of protein expressions destined for the outer segment may contribute to the rapid rod death observed in the *rh1–1* mutants. In contrast, in the mouse, the expression of rod-specific transcription factors occurs after terminal mitosis [99], and the Rho expression for later-born rod precursors is delayed for 5.5–6.5 days following terminal mitosis [100]. The rapid degeneration in zebrafish may prove advantageous as a model for high-throughput in-vivo drug screens to identify small molecules that may slow the degeneration phenotype.

A recent report by Feehan et al. [30] uses a similar gene-targeting approach to generate endogenous mutations in the *Xenopus rho* genes, and they found phenotypes consistent with dominant and recessive forms of RP, including rod cell loss and opsin mislocalization. *X. laevis* are tetraploid organisms, and the three Rho gene products are highly conserved, with either silent or conservative amino acid differences among them. Rod degeneration was associated with larger in-frame indels; however, frame shift mutations or loss of the initiation methionine, resulting in a lower opsin expression, were not associated with degeneration. The zebrafish *rh1–2* amino acid sequence is 78% conserved with zebrafish *rh1–1*, with a putative N-linked glycosylation consensus sequence at N15 (NES compared with NAT in Rho), but no C-terminal VXPX sorting signal. Unlike *rh1–1*, the *rh1–2* expression is delayed until 5 dpf, at which time the expression is restricted to the ONL adjacent to the peripheral retina, where it remains at 175 dpf [79,80]. Our data for gene targeting *rh1–2* did not reveal any rod degeneration (data not shown). Furthermore, the rod death in our putative null allele of *rh1–1* suggests the absence of genetic compensatory effects, consistent with the late onset and limited expression pattern of *rh1–2*.

In summary, we have taken advantage of recent advances in genome editing to generate novel alleles of the zebrafish *rh1–1* locus, which displays inheritance patterns and molecular features similar to major classes of human alleles associated with disease. Moreover, histological analyses showed patterns of rod dysfunction and degeneration analogous to those contributing to human RP. These lines provide a small yet useful collection of zebrafish models for use in high-throughput in-vivo small molecule screens or genetic screens to identify compounds or gene targets to slow the rod degeneration associated with RP.

ACKNOWLEDGMENTS

This work was supported by grants funded by the Foundation Fighting Blindness, TA-NMT-0614–0654-FSU, and The National Institutes of Health R21EY025410. We thank the members of the Fadool laboratory. We thank the staff of the Department of Biological Science Imaging Resource Facility, and Sequencing and Molecular Cloning Laboratory and the University of Utah Mutation Generation and Detection Core for their assistance designing and constructing the gRNA targeting vectors.

REFERENCES

1. Sullivan LS, Bowne SJ, Birch DG, Hughbanks-Wheaton D, Heckenlively JR, Lewis RA, Garcia CA, Ruiz RS, Blanton SH, Northrup H, Gire AI, Seaman R, Duzkale H, Spellicy CJ, Zhu J, Shankar SP, Daiger SP. Prevalence of disease-causing mutations in families with autosomal dominant retinitis pigmentosa: A screen of known genes in 200 families. Invest Ophthalmol Vis Sci 2006; 47:3052-64. [PMID: 16799052].
2. Sung CH, Davenport CM, Nathans J. Rhodopsin mutations responsible for autosomal dominant retinitis pigmentosa. clustering of functional classes along the polypeptide chain. J Biol Chem 1993; 268:26645-9. [PMID: 8253795].
3. Sung CH, Schneider BG, Agarwal N, Papermaster DS, Nathans J. Functional heterogeneity of mutant rhodopsins responsible for autosomal dominant retinitis pigmentosa. Proc Natl Acad Sci USA 1991; 88:8840-4. [PMID: 1924344].
4. Kaushal S, Ridge KD, Khorana HG. Structure and function in rhodopsin: The role of asparagine-linked glycosylation. Proc Natl Acad Sci USA 1994; 91:4024-8. [PMID: 8171029].
5. Chuang JZ, Vega C, Jun W, Sung CH. Structural and functional impairment of endocytic pathways by retinitis pigmentosa mutant rhodopsin-arrestin complexes. J Clin Invest 2004; 114:131-40. [PMID: 15232620].
6. Cideciyan AV, Hood DC, Huang Y, Banin E, Li ZY, Stone EM, Milam AH, Jacobson SG. Disease sequence from mutant rhodopsin allele to rod and cone photoreceptor degeneration in man. Proc Natl Acad Sci USA 1998; 95:7103-8. [PMID: 9618546].
7. Mendes HF, van der Spuy J, Chapple JP, Cheetham ME. Mechanisms of cell death in rhodopsin retinitis pigmentosa: Implications for therapy. Trends Mol Med 2005; 11:177-85. [PMID: 15823756].
8. Deretic D, Schmerl S, Hargrave PA, Arendt A, McDowell JH. Regulation of sorting and post-golgi trafficking of rhodopsin by its C-terminal sequence QVS(A)PA. Proc Natl Acad Sci USA 1998; 95:10620-5. [PMID: 9724753].
9. Tam BM, Moritz OL, Hurd LB, Papermaster DS. Identification of an outer segment targeting signal in the COOH terminus of rhodopsin using transgenic xenopus laevis. J Cell Biol 2000; 151:1369-80. [PMID: 11134067].
10. Chen J, Makino CL, Peachey NS, Baylor DA, Simon MI. Mechanisms of rhodopsin inactivation in vivo as revealed by a COOH-terminal truncation mutant. Science 1995; 267:374-7. [PMID: 7824934].
11. Dryja TP, Hahn LB, Cowley GS, McGee TL, Berson EL. Mutation spectrum of the rhodopsin gene among patients with autosomal dominant retinitis pigmentosa. Proc Natl Acad Sci USA 1991; 88:9370-4. [PMID: 1833777].
12. Dryja TP, McGee TL, Hahn LB, Cowley GS, Olsson JE, Reichel E, Sandberg MA, Berson EL. Mutations within the rhodopsin gene in patients with autosomal dominant retinitis pigmentosa. N Engl J Med 1990; 323:1302-7. [PMID: 2215617].
13. Dryja TP, McGee TL, Reichel E, Hahn LB, Cowley GS, Yandell DW, Sandberg MA, Berson EL. A point mutation of the rhodopsin gene in one form of retinitis pigmentosa. Nature 1990; 343:364-6. [PMID: 2137202].
14. Stone EM, Kimura AE, Nichols BE, Khadivi P, Fishman GA, Sheffield VC. Regional distribution of retinal degeneration in patients with the proline to histidine mutation in codon 23 of the rhodopsin gene. Ophthalmology 1991; 98:1806-13. [PMID: 1775314].
15. John SK, Smith JE, Aguirre GD, Milam AH. Loss of cone molecular markers in rhodopsin-mutant human retinas with retinitis pigmentosa. Mol Vis 2000; 6:204-15. [PMID: 11063754].
16. Hargrave PA. The N-terminal tryptic peptide of bovine rhodopsin. A glycopeptide containing two sites of oligosaccharide attachment. Biochim Biophys Acta 1977; 492:83-94. [PMID: 861254].
17. Sullivan LJ, Makris GS, Dickinson P, Mulhall LE, Forrest S, Cotton RG, Loughnan MS. A new codon 15 rhodopsin gene mutation in autosomal dominant retinitis pigmentosa is associated with sectorial disease. Arch Ophthalmol 1993; 111:1512-7. [PMID: 8240107].
18. Fishman GA, Stone EM, Sheffield VC, Gilbert LD, Kimura AE. Ocular findings associated with rhodopsin gene codon 17 and codon 182 transition mutations in dominant retinitis pigmentosa. Arch Ophthalmol 1992; 110:54-62. [PMID: 1731723].
19. Keeler C. Retinal degeneration in the mouse is rodless retina. J Hered 1966; 57:47-50. [PMID: 5916892].
20. van Nie R, Ivanyi D, Demant P. A new H-2-linked mutation, rds, causing retinal degeneration in the mouse. Tissue Antigens 1978; 12:106-8. [PMID: 705766].
21. Drager UC, Hubel DH. Studies of visual function and its decay in mice with hereditary retinal degeneration. J Comp Neurol 1978; 180:85-114. [PMID: 649791].
22. Chang B, Hawes NL, Pardue MT, German AM, Hurd RE, Davisson MT, Nusinowitz S, Rengarajan K, Boyd AP, Sidney SS, Phillips MJ, Stewart RE, Chaudhury R, Nickerson JM, Heckenlively JR, Boatright JH. Two mouse retinal degenerations caused by missense mutations in the beta-subunit of rod cGMP phosphodiesterase gene. Vision Res 2007; 47:624-33. [PMID: 17267005].
23. Bourne MC, Campbell DA, Tansley K. Hereditary degeneration of the rat retina. Br J Ophthalmol 1938; 22:613-23. [PMID: 18169569].
24. D'Cruz PM, Yasumura D, Weir J, Matthes MT, Abderrahim H, LaVail MM, Vollrath D. Mutation of the receptor tyrosine kinase gene mertk in the retinal dystrophic RCS rat. Hum Mol Genet 2000; 9:645-51. [PMID: 10699188].
25. Gal A, Li Y, Thompson DA, Weir J, Orth U, Jacobson SG, Apfelstedt-Sylla E, Vollrath D. Mutations in MERTK, the human orthologue of the RCS rat retinal dystrophy gene, cause retinitis pigmentosa. Nat Genet 2000; 26:270-1. [PMID: 11062461].

26. Olsson JE, Gordon JW, Pawlyk BS, Roof D, Hayes A, Molday RS, Mukai S, Cowley GS, Berson EL, Dryja TP. Transgenic mice with a rhodopsin mutation (Pro23His): A mouse model of autosomal dominant retinitis pigmentosa. Neuron 1992; 9:815-30. [PMID: 1418997].

27. Petters RM, Alexander CA, Wells KD, Collins EB, Sommer JR, Blanton MR, Rojas G, Hao Y, Flowers WL, Banin E, Cideciyan AV, Jacobson SG, Wong F. Genetically engineered large animal model for studying cone photoreceptor survival and degeneration in retinitis pigmentosa. Nat Biotechnol 1997; 15:965-70. [PMID: 9335046].

28. Tam BM, Moritz OL. Characterization of rhodopsin P23H-induced retinal degeneration in a xenopus laevis model of retinitis pigmentosa. Invest Ophthalmol Vis Sci 2006; 47:3234-41. [PMID: 16877386].

29. Tam BM, Moritz OL. Dark rearing rescues P23H rhodopsin-induced retinal degeneration in a transgenic xenopus laevis model of retinitis pigmentosa: A chromophore-dependent mechanism characterized by production of N-terminally truncated mutant rhodopsin. J Neurosci 2007; 27:9043-53. [PMID: 17715341].

30. Tam BM, Moritz OL. The role of rhodopsin glycosylation in protein folding, trafficking, and light-sensitive retinal degeneration. J Neurosci 2009; 29:15145-54. [PMID: 19955366].

31. Tam BM, Noorwez SM, Kaushal S, Kono M, Moritz OL. Photoactivation-induced instability of rhodopsin mutants T4K and T17M in rod outer segments underlies retinal degeneration in X. laevis transgenic models of retinitis pigmentosa. J Neurosci 2014; 34:13336-48. [PMID: 25274813].

32. Tam BM, Xie G, Oprian DD, Moritz OL. Mislocalized rhodopsin does not require activation to cause retinal degeneration and neurite outgrowth in xenopus laevis. J Neurosci 2006; 26:203-9. [PMID: 16399688].

33. Naash MI, Hollyfield JG, al-Ubaidi MR, Baehr W. Simulation of human autosomal dominant retinitis pigmentosa in transgenic mice expressing a mutated murine opsin gene. Proc Natl Acad Sci USA 1993; 90:5499-503. [PMID: 8516292].

34. Martinez-Navarrete G, Seiler MJ, Aramant RB, Fernandez-Sanchez L, Pinilla I, Cuenca N. Retinal degeneration in two lines of transgenic S334ter rats. Exp Eye Res 2011; 92:227-37. [PMID: 21147100].

35. Scott PA, de Castro JP, DeMarco PJ, Ross JW, Njoka J, Walters E, Prather RS, McCall MA, Kaplan HJ. Progression of Pro23His retinopathy in a miniature swine model of retinitis pigmentosa. Transl Vis Sci Technol 2017; 6:4-[PMID: 28316877].

36. Li T, Sandberg MA, Pawlyk BS, Rosner B, Hayes KC, Dryja TP, Berson EL. Effect of vitamin A supplementation on rhodopsin mutants threonine-17–> methionine and proline-347–> serine in transgenic mice and in cell cultures. Proc Natl Acad Sci USA 1998; 95:11933-8. [PMID: 9751768].

37. Orhan E, Dalkara D, Neuille M, Lechauve C, Michiels C, Picaud S, Leveillard T, Sahel JA, Naash MI, Lavail MM, Zeitz C, Audo I. Genotypic and phenotypic characterization of P23H line 1 rat model. PLoS One 2015; 10:e0127319-[PMID: 26009893].

38. Aguirre GD. Concepts and strategies in retinal gene therapy. Invest Ophthalmol Vis Sci 2017; 58:5399-411. [PMID: 29053763].

39. Aguirre GD. Animal models as tools for screening candidate drugs. Retina 2005; 25:S36-7. [PMID: 16374326].

40. Aquirre G, Farber D, Lolley R, Fletcher RT, Chader GJ. Rod-cone dysplasia in irish setters: A defect in cyclic GMP metabolism in visual cells. Science 1978; 201:1133-4. [PMID: 210508].

41. Kijas JW, Cideciyan AV, Aleman TS, Pianta MJ, Pearce-Kelling SE, Miller BJ, Jacobson SG, Aguirre GD, Acland GM. Naturally occurring rhodopsin mutation in the dog causes retinal dysfunction and degeneration mimicking human dominant retinitis pigmentosa. Proc Natl Acad Sci USA 2002; 99:6328-33. [PMID: 11972042].

42. Jones BW, Kondo M, Terasaki H, Watt CB, Rapp K, Anderson J, Lin Y, Shaw MV, Yang JH, Marc RE. Retinal remodeling in the tg P347L rabbit, a large-eye model of retinal degeneration. J Comp Neurol 2011; 519:2713-33. [PMID: 21681749].

43. Sung CH, Makino C, Baylor D, Nathans J. A rhodopsin gene mutation responsible for autosomal dominant retinitis pigmentosa results in a protein that is defective in localization to the photoreceptor outer segment. J Neurosci 1994; 14:5818-33. [PMID: 7523628].

44. Green ES, Menz MD, LaVail MM, Flannery JG. Characterization of rhodopsin mis-sorting and constitutive activation in a transgenic rat model of retinitis pigmentosa. Invest Ophthalmol Vis Sci 2000; 41:1546-53. [PMID: 10798675].

45. LaVail MM, Nishikawa S, Steinberg RH, Naash MI, Duncan JL, Trautmann N, Matthes MT, Yasumura D, Lau-Villacorta C, Chen J, Peterson WM, Yang H, Flannery JG. Phenotypic characterization of P23H and S334ter rhodopsin transgenic rat models of inherited retinal degeneration. Exp Eye Res 2018; 167:56-90. [PMID: 29122605].

46. Hombrebueno JR, Tsai MM, Kim HL, De Juan J, Grzywacz NM, Lee EJ. Morphological changes of short-wavelength cones in the developing S334ter-3 transgenic rat. Brain Res 2010; 1321:60-6. [PMID: 20114037].

47. Sandoval IM, Price BA, Gross AK, Chan F, Sammons JD, Wilson JH, Wensel TG. Abrupt onset of mutations in a developmentally regulated gene during terminal differentiation of post-mitotic photoreceptor neurons in mice. PLoS One 2014; 9:e108135-[PMID: 25264759].

48. Sakami S, Kolesnikov AV, Kefalov VJ, Palczewski K. P23H opsin knock-in mice reveal a novel step in retinal rod disc morphogenesis. Hum Mol Genet 2014; 23:1723-41. [PMID: 24214395].

49. Sakami S, Maeda T, Bereta G, Okano K, Golczak M, Sumaroka A, Roman AJ, Cideciyan AV, Jacobson SG, Palczewski K. Probing mechanisms of photoreceptor degeneration in a new mouse model of the common form of autosomal

dominant retinitis pigmentosa due to P23H opsin mutations. J Biol Chem 2011; 286:10551-67. [PMID: 21224384].

50. Price BA, Sandoval IM, Chan F, Simons DL, Wu SM, Wensel TG, Wilson JH. Mislocalization and degradation of human P23H-rhodopsin-GFP in a knockin mouse model of retinitis pigmentosa. Invest Ophthalmol Vis Sci 2011; 52:9728-36. [PMID: 22110080].

51. Feehan JM, Chiu CN, Stanar P, Tam BM, Ahmed SN, Moritz OL. Modeling dominant and recessive forms of retinitis pigmentosa by editing three rhodopsin-encoding genes in xenopus laevis using Crispr/Cas9. Sci Rep 2017; 7:6920-.

52. Malicki J, Neuhauss SC, Schier AF, Solnica-Krezel L, Stemple DL, Stainier DY, Abdelilah S, Zwartkruis F, Rangini Z, Driever W. Mutations affecting development of the zebrafish retina. Development 1996; 123:263-73. [PMID: 9007246].

53. Brockerhoff SE, Hurley JB, Janssen-Bienhold U, Neuhauss SC, Driever W, Dowling JE. A behavioral screen for isolating zebrafish mutants with visual system defects. Proc Natl Acad Sci USA 1995; 92:10545-9. [PMID: 7479837].

54. Fadool JM, Brockerhoff SE, Hyatt GA, Dowling JE. Mutations affecting eye morphology in the developing zebrafish (danio rerio). Dev Genet 1997; 20:288-95. [PMID: 9216068].

55. Fadool JM, Dowling JE. Zebrafish: A model system for the study of eye genetics. Prog Retin Eye Res 2008; 27:89-110. [PMID: 17962065].

56. Gross JM, Perkins BD. Zebrafish mutants as models for congenital ocular disorders in humans. Mol Reprod Dev 2008; 75:547-55. [PMID: 18058918].

57. Alvarez-Delfin K, Morris AC, Snelson CD, Gamse JT, Gupta T, Marlow FL, Mullins MC, Burgess HA, Granato M, Fadool JM. Tbx2b is required for ultraviolet photoreceptor cell specification during zebrafish retinal development. Proc Natl Acad Sci USA 2009; 106:2023-8. [PMID: 19179291].

58. Saade CJ, Alvarez-Delfin K, Fadool JM. Rod photoreceptors protect from cone degeneration-induced retinal remodeling and restore visual responses in zebrafish. J Neurosci 2013; 33:1804-14. [PMID: 23365220].

59. Morris AC, Schroeter EH, Bilotta J, Wong RO, Fadool JM. Cone survival despite rod degeneration in XOPS-mCFP transgenic zebrafish. Invest Ophthalmol Vis Sci 2005; 46:4762-71. [PMID: 16303977].

60. Morris AC, Scholz TL, Brockerhoff SE, Fadool JM. Genetic dissection reveals two separate pathways for rod and cone regeneration in the teleost retina. Dev Neurobiol 2008; 68:605-19. [PMID: 18265406].

61. Montgomery JE, Parsons MJ, Hyde DR. A novel model of retinal ablation demonstrates that the extent of rod cell death regulates the origin of the regenerated zebrafish rod photoreceptors. J Comp Neurol 2010; 518:800-14. [PMID: 20058308].

62. Stearns G, Evangelista M, Fadool JM, Brockerhoff SE. A mutation in the cone-specific pde6 gene causes rapid cone photoreceptor degeneration in zebrafish. J Neurosci 2007; 27:13866-74. [PMID: 18077698].

63. Sotolongo-Lopez M, Alvarez-Delfin K, Saade CJ, Vera DL, Fadool JM. Genetic dissection of dual roles for the transcription factor six7 in photoreceptor development and patterning in zebrafish. PLoS Genet 2016; 12:e1005968-[PMID: 27058886].

64. Lewis TR, Kundinger SR, Pavlovich AL, Bostrom JR, Link BA, Besharse JC. Cos2/Kif7 and osm-3/Kif17 regulate onset of outer segment development in zebrafish photoreceptors through distinct mechanisms. Dev Biol 2017; 425:176-90. [PMID: 28341548].

65. Taylor SM, Alvarez-Delfin K, Saade CJ, Thomas JL, Thummel R, Fadool JM, Hitchcock PF. The bHLH transcription factor NeuroD governs photoreceptor genesis and regeneration through delta-notch signaling. Invest Ophthalmol Vis Sci 2015; 56:7496-515. [PMID: 26580854].

66. Auer TO, Duroure K, De Cian A, Concordet JP, Del Bene F. Highly efficient CRISPR/Cas9-mediated knock-in in zebrafish by homology-independent DNA repair. Genome Res 2014; 24:142-53. [PMID: 24179142].

67. Kimura Y, Hisano Y, Kawahara A, Higashijima S. Efficient generation of knock-in transgenic zebrafish carrying reporter/driver genes by CRISPR/Cas9-mediated genome engineering. Sci Rep 2014; 4:6545-[PMID: 25293390].

68. Hwang WY, Fu Y, Reyon D, Maeder ML, Kaini P, Sander JD, Joung JK, Peterson RT, Yeh JR. Heritable and precise zebrafish genome editing using a CRISPR-cas system. PLoS One 2013; 8:e68708-[PMID: 23874735].

69. Irion U, Krauss J, Nusslein-Volhard C. Precise and efficient genome editing in zebrafish using the CRISPR/Cas9 system. Development 2014; 141:4827-30. [PMID: 25411213].

70. Armstrong GA, Liao M, You Z, Lissouba A, Chen BE, Drapeau P. Homology directed knockin of point mutations in the zebrafish tardbp and fus genes in ALS using the CRISPR/Cas9 system. PLoS One 2016; 11:e0150188-[PMID: 26930076].

71. Lessieur EM, Fogerty J, Gaivin RJ, Song P, Perkins BD. The ciliopathy gene ahi1 is required for zebrafish cone photoreceptor outer segment morphogenesis and survival. Invest Ophthalmol Vis Sci 2017; 58:448-60. [PMID: 28118669].

72. Van De Weghe JC, Rusterholz TDS, Latour B, Grout ME, Aldinger KA, Shaheen R, Dempsey JC, Maddirevula S, Cheng YH, Phelps IG, Gesemann M, Goel H, Birk OS, Alanzi T, Rawashdeh R, Khan AO. University of Washington Center for Mendelian Genomics, Bamshad MJ, Nickerson DA, Neuhauss SCF, Dobyns WB, Alkuraya FS, Roepman R, Bachmann-Gagescu R, Doherty D. Mutations in ARMC9, which encodes a basal body protein, cause joubert syndrome in humans and ciliopathy phenotypes in zebrafish. Am J Hum Genet 2017; 101:23-36. [PMID: 28625504].

73. Westerfield M. The Zebrafish Book; A guide for the laboratory use of zebrafish (Danio rerio). 4th ed. Eugene (OR): University of Oregon Press; 2000.

74. Fadool JM. Development of a rod photoreceptor mosaic revealed in transgenic zebrafish. Dev Biol 2003; 258:277-90. [PMID: 12798288].

75. Ile KE, Kassen S, Cao C, Vihtehlic T, Shah SD, Mousley CJ, Alb JG Jr, Huijbregts RP, Stearns GW, Brockerhoff SE, Hyde DR, Bankaitis VA. Zebrafish class 1 phosphatidylinositol transfer proteins: PITPbeta and double cone cell outer segment integrity in retina. Traffic 2010; 11:1151-67. [PMID: 20545905].

76. Larison KD, Bremiller R. Early onset of phenotype and cell patterning in the embryonic zebrafish retina. Development 1990; 109:567-76. [PMID: 2401210].

77. Fadool JM, Linser PJ. Differential glycosylation of the 5A11/HT7 antigen by neural retina and epithelial tissues in the chicken. J Neurochem 1993; 60:1354-64. [PMID: 8455029].

78. Velez P, Schwartz AB, Iyer SR, Warrington A, Fadool DA. Ubiquitin ligase Nedd4–2 modulates Kv1.3 current amplitude and ion channel protein targeting. J Neurophysiol 2016; 116:671-85. [PMID: 27146988].

79. Morrow JM, Lazic S, Chang BS. A novel rhodopsin-like gene expressed in zebrafish retina. Vis Neurosci 2011; 28:325-35. [PMID: 21447259].

80. Morrow JM, Lazic S, Dixon Fox M, Kuo C, Schott RK. de A Gutierrez E, Santini F, Tropepe V, Chang BS. A second visual rhodopsin gene, rh1–2, is expressed in zebrafish photoreceptors and found in other ray-finned fishes. J Exp Biol 2017; 220:294-303. [PMID: 27811293].

81. Lem J, Krasnoperova NV, Calvert PD, Kosaras B, Cameron DA, Nicolo M, Makino CL, Sidman RL. Morphological, physiological, and biochemical changes in rhodopsin knockout mice. Proc Natl Acad Sci USA 1999; 96:736-41. [PMID: 9892703].

82. Stenkamp DL. Neurogenesis in the fish retina. Int Rev Cytol 2007; 259:173-224. [PMID: 17425942].

83. Hartong DT, Berson EL, Dryja TP. Retinitis pigmentosa. Lancet 2006; 368:1795-809. [PMID: 17113430].

84. Rosenfeld PJ, Cowley GS, McGee TL, Sandberg MA, Berson EL, Dryja TP. A null mutation in the rhodopsin gene causes rod photoreceptor dysfunction and autosomal recessive retinitis pigmentosa. Nat Genet 1992; 1:209-13. [PMID: 1303237].

85. Humphries MM, Rancourt D, Farrar GJ, Kenna P, Hazel M, Bush RA, Sieving PA, Sheils DM, McNally N, Creighton P, Erven A, Boros A, Gulya K, Capecchi MR, Humphries P. Retinopathy induced in mice by targeted disruption of the rhodopsin gene. Nat Genet 1997; 15:216-9. [PMID: 9020854].

86. Frederick JM, Krasnoperova NV, Hoffmann K, Church-Kopish J, Ruther K, Howes K, Lem J, Baehr W. Mutant rhodopsin transgene expression on a null background. Invest Ophthalmol Vis Sci 2001; 42:826-33. [PMID: 11222546].

87. Concepcion F, Chen J. Q344ter mutation causes mislocalization of rhodopsin molecules that are catalytically active: A mouse model of Q344ter-induced retinal degeneration. PLoS One 2010; 5:e10904-[PMID: 20532191].

88. Nelson SM, Frey RA, Wardwell SL, Stenkamp DL. The developmental sequence of gene expression within the rod photoreceptor lineage in embryonic zebrafish. Dev Dyn 2008; 237:2903-17. [PMID: 18816851].

89. Chen J, Rattner A, Nathans J. The rod photoreceptor-specific nuclear receptor Nr2e3 represses transcription of multiple cone-specific genes. J Neurosci 2005; 25:118-29. [PMID: 15634773].

90. Suzuki SC, Bleckert A, Williams PR, Takechi M, Kawamura S, Wong RO. Cone photoreceptor types in zebrafish are generated by symmetric terminal divisions of dedicated precursors. Proc Natl Acad Sci USA 2013; 110:15109-14. [PMID: 23980162].

91. Raymond PA, Barthel LK, Curran GA. Developmental patterning of rod and cone photoreceptors in embryonic zebrafish. J Comp Neurol 1995; 359:537-50. [PMID: 7499546].

92. Hu M, Easter SS. Retinal neurogenesis: The formation of the initial central patch of postmitotic cells. Dev Biol 1999; 207:309-21. [PMID: 10068465].

93. Schmitt EA, Dowling JE. Comparison of topographical patterns of ganglion and photoreceptor cell differentiation in the retina of the zebrafish, danio rerio. J Comp Neurol 1996; 371:222-34. [PMID: 8835728].

94. Robinson J, Schmitt EA, Dowling JE. Temporal and spatial patterns of opsin gene expression in zebrafish (danio rerio). Vis Neurosci 1995; 12:895-906. [PMID: 8924413].

95. Schmitt EA, Dowling JE. Early retinal development in the zebrafish, danio rerio: Light and electron microscopic analyses. J Comp Neurol 1999; 404:515-36. [PMID: 9987995].

96. Branchek T, Bremiller R. The development of photoreceptors in the zebrafish, brachydanio rerio. I. structure. J Comp Neurol 1984; 224:107-15. [PMID: 6715574].

97. Branchek T. The development of photoreceptors in the zebrafish, brachydanio rerio. II. function. J Comp Neurol 1984; 224:116-22. [PMID: 6715575].

98. Easter SS Jr, Nicola GN. The development of vision in the zebrafish (danio rerio). Dev Biol 1996; 180:646-63. [PMID: 8954734].

99. Akimoto M, Cheng H, Zhu D, Brzezinski JA, Khanna R, Filippova E, Oh EC, Jing Y, Linares JL, Brooks M, Zareparsi S, Mears AJ, Hero A, Glaser T, Swaroop A. Targeting of GFP to newborn rods by nrl promoter and temporal expression profiling of flow-sorted photoreceptors. Proc Natl Acad Sci USA 2006; 103:3890-5. [PMID: 16505381].

100. Morrow EM, Belliveau MJ, Cepko CL. Two phases of rod photoreceptor differentiation during rat retinal development. J Neurosci 1998; 18:3738-48. [PMID: 9570804].

Articles are provided courtesy of Emory University and the Zhongshan Ophthalmic Center, Sun Yat-sen University, P.R. China. The print version of this article was created on 27 August 2018. This reflects all typographical corrections and errata to the article through that date. Details of any changes may be found in the online version of the article.